Numerical analysis of ionic mass transfer in the electrolytic bath of an aluminium reduction cell

Mohsen Ariana[1], Martin Désilets[1], Pierre Proulx[2]
Mechanical engineering department, Universite de Sherbrooke, 2500, Boul. de l'Université, Sherbrooke, Québec, Canada
Chemical engineering department, Universite de Sherbrooke, 2500, Boul. de l'Université, Sherbrooke, Québec, Canada

Keywords: Mass transfer, bath, concentration profiles, migration, diffusion.

Abstract

In the Hall-Héroult process, the electrolytic bath is a molten solution of cryolite and alumina. Like all other molten salts, it ends up in different moving ions driven by physical mechanisms such as convection, diffusion and migration. The motion of these ions and their concentration distribution are important because they determine many functional macroscopic parameters of the electrolytic cell like current density distribution, heat generation, back reactions, current efficiency, and mass-transfer controlled reactions at the electrodes. In this study, a numerical model for the fluxes of most important ions in a NaF-AlF_3-Al_2O_3 system has been proposed. The reactions in the bath and the resulted ions have been added to the reactions that take place at the cathode and anode, and a finite element model has been presented for the electrolyte portion of the aluminium reduction cell. The transient motion of the different ions under the migration and diffusion mechanisms have been modelled based on the classical mass transfer equations. The results illustrate the significant role of the migration in the early stages of electrochemical process. This mechanism is also the dominating effect in the motion of nonelectroactive species. For larger time scales, because of the depletion of the consumed species and accumulation of the produced species near the electrodes, the mass transfer is dominated by the diffusion.

Introduction

In the Hall-Héroult production process, the aluminium ore is dissolved in molten cryolite. This molten solution, called the bath, is composed of different charged ions moving in an electric field, a few of them being involved in the reactions at electrodes. Most of them can be considered as rapid reactions due to the high temperature prevailing inside the cells. However, the flux of ions that has an important impact on the electrochemical reactions since the motion of these ions is at the origin of the mass transfer controlled reactions. Also, another important functional parameter of the cell, the current efficiency, is greatly influenced by the species mass transfer. It is well known that current efficiency is inversely proportional to the rate of back reaction (1). The source of the back reaction is the chemical dissolution of aluminium in the bath, its mass transfer toward the anode and finally its oxidation by CO_2 (1). From this point of view, defining the mass transfer mechanisms can be viewed as the fundamental analysis of the loss of current efficiency in the bath.

Despite the importance of the current density and the mass transfer controlled reaction at the anode and cathode, the experimental measurement of the flux or concentration of these ions is very difficult due to high temperature and harsh conditions inside the electrolysis cell (1, 2). The driving forces for the different mechanisms of ionic mass transfer are either the electric field or the concentration gradient of each ion in the bath. The convection also plays an important role in the mixing of these ions.

Modeling of the mass transfer in the cell thus couples four different fields: electric, concentration, velocity and temperature fields. There have been many modeling studies dedicated to the analysis of several of these fields. Zoric et al. (3-5) modeled the electric potential and current densities in the cell by applying the secondary current distribution assumption for a two dimensional cell. More recently, Solheim (6) predicted the mass fractions of NaF, AlF_3, Al_2O_3, and CaF_2 in order to analyze the rate of cryolite crystallization. His model is based on the resolution of the Maxwell-Stefan diffusion equation for different ions in the bath near the cathode (7). Gagnon et al. solved the coupled Nernst-Planck and Poisson's equations to simulate the ions concentration near the cathode for a NaF-AlF_3 electrolyte (8). These two latter studies are the most recent works on mass transfer modeling in an aluminium reduction cell. There have been other studies focusing on the convection and mass transfer in the cell, however, these studies are not considering ions in the cell nor the motion of these ions based on migration or diffusion mechanisms (9-11).
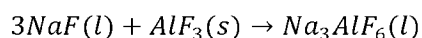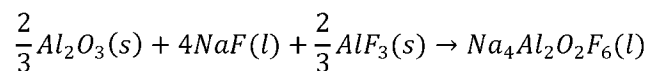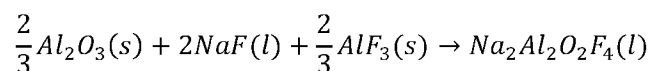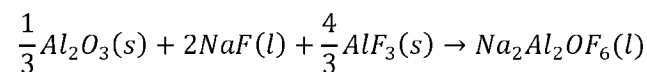
For the first time in this study, the mass transfer of charged ions in a NaF-AlF_3-Al_2O_3 mixture is predicted by considering diffusion, migration, and electrochemical reaction at both electrodes, in a full cell model.
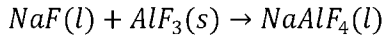
Model

The ionic composition of bath is a controversial subject. In fact, the ions and complexes in the bath are not completely defined yet and different ionic equilibriums have been proposed. In addition, the reactions that take place at the electrodes are not well defined (1, 2). This situation certainly explains some of the difficulties inherent to the development of a whole-cell mass transfer model.

Homogeneous reactions
The initial composition of bath is based on the dissolution of alumina in cryolite, as modeled by Zhang et Rapp (9). These authors consider five simultaneous reactions and five products, as it is shown below:

$$\frac{1}{3}Al_2O_3(s) + 2NaF(l) + \frac{4}{3}AlF_3(s) \rightarrow Na_2Al_2OF_6(l)$$

$$\frac{2}{3}Al_2O_3(s) + 2NaF(l) + \frac{2}{3}AlF_3(s) \rightarrow Na_2Al_2O_2F_4(l)$$

$$\frac{2}{3}Al_2O_3(s) + 4NaF(l) + \frac{2}{3}AlF_3(s) \rightarrow Na_4Al_2O_2F_6(l)$$

$$3NaF(l) + AlF_3(s) \rightarrow Na_3AlF_6(l)$$

$$NaF(l) + AlF_3(s) \rightarrow NaAlF_4(l)$$

The molar fractions of the above species are calculated by considering the activities of Al_2O_3, AlF_3, and NaF given by the following relations:

$$[Na_2Al_2OF_6] = K_1 a_{NaF}{}^2 a_{AlF_3}{}^{\frac{4}{3}} a_{Al_2O_3}{}^{\frac{1}{3}}$$

$$[Na_2Al_2O_2F_4] = K_2 a_{NaF}{}^2 a_{AlF_3}{}^{2/3} a_{Al_2O_3}{}^{2/3}$$

$$[Na_4Al_2O_2F_6] = K_3 a_{NaF}{}^4 a_{AlF_3}{}^{2/3} a_{Al_2O_3}{}^{2/3}$$

$$[Na_3AlF_6] = K_4 a_{NaF}{}^3 a_{AlF_3}$$

$$[NaAlF_4] = K_5 a_{NaF} a_{AlF_3}$$

Where K_i are the equilibrium constants, and a_{NaF}, a_{AlF3}, and a_{Al2O3} are the activity of NaF, AlF_3, and Al_2O_3 respectively. Moreover, the value of activities and equilibrium constants are functions of temperature and cryolite ratio, as given by Zhang et Rapp (12). It should be noted that bath is assumed to be saturated in alumina. In consequence, the activity of alumina is equal to unity (13).

It is well known that the only cation in the system is Na^+, in such amount that it surrounds all other anions (1). Therefore, in this study, it is assumed that the complexes on the right hand side of above reactions directly dissociate into Na+ ions and its corresponding anion.
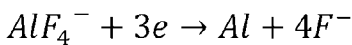
Heterogeneous reactions
There have been several mechanisms proposed for reactions that take place at the electrodes (1, 2). In this study, a single one step reaction is assumed at both electrodes.

The anodic reaction is given as:

$$2Al_2OF_6{}^{-2} + 4F^- + C \rightarrow 4AlF_4{}^- + CO_2 + 4e$$
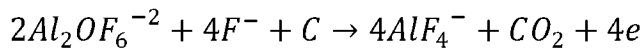
While for the cathode, the reaction can be expressed as:

$$AlF_4{}^- + 3e \rightarrow Al + 4F^-$$

In other words, $Al_2OF_6{}^{-2}$ is consumed at the anode, thereby producing $AlF_4{}^-$. This last species will then move to the cathode by diffusion, where it will be reduced to produce aluminium. The produced F^- ions diffuse and migrate to the anode to participate in the anodic reaction. One by-product of the anodic reaction is CO_2. It is assumed here that it will leave the system without affecting the mass transfer of all other components.

Reaction kinetics
As stated before, electric forces and concentration gradients are the two mechanisms of the ionic mass transfer considered. To evaluate the electric field and consequently the current density, Poisson's equation should be solved in the electrolyte:

$$\nabla^2 \phi = -\frac{\rho_E}{\varepsilon \varepsilon_0}$$

Where Φ, is the potential, ρ_E the electric charge density (C.m-3), ε_0 the electric permittivity of vacuum, and ε the static dielectric constant (or relative electric permittivity).

The boundary condition on each electrode is defined with the electric potential as a function of the current density, based on the corresponding reaction kinetics.

For the anodic reaction, a Tafel equation, which is a logarithmic approximation of the Butler-Volmer equation, is proposed (14):

$$\varphi_A^S = U_{cell} - E_{rev,A} - a_A - b_A log(j)$$

Where $E_{rev,A}$ is equal to 1.23 V; a_A and b_A are the Tafel parameters, taken as 0.5 V and 0.25 V.decade^{-1} respectively. j finally represents the current density.

For the cathode reaction, a linearized Butler-Volmer equation is applicable:

$$E_C = -E_{rev,C} - b_C |j|$$

Where $E_{rev,A}$ is equal to zero for cathodic reaction and b_c is taken as 0.008 Ω.cm^2.

Mass transfer model
The prediction of the mass transfer of different ions is based on classical mass conservation equation for each species, as given below:

$$\frac{\partial w_i}{\partial t} + \nabla N_i + R_i = 0$$

Where w_i, N_i and R_i represent mass fraction, mass flux, and the reaction rate for species I, respectively. The flux of species for a concentrated solution is driven by the electric forces acting on charged species and also by the concentration gradients, as given by the following equation:

$$Ni = -(\rho D_i \nabla w_i + \rho w_i D_i \frac{\nabla M_n}{M_n} + \rho w_i z_i u_i \nabla \phi)$$

Where ρ_i, D_i, M_n, z_i, and u_i are the density, mass diffusivity, mean molar mass fraction, charge number, and mobility, respectively.

The boundary conditions for this equation can be given by the famous Butler-Volmer equation for two categories of ions based on their participation in the reaction:

For nonelectroactive ions:

$$N_i = 0$$

And for electroactive ions:

$$N_i = \frac{\nu_i}{nF} j$$

Where n is the number of electron transferred and ν_i is the stoichiometric coefficient in the corresponding reaction, and F the Faraday's constant.

Additional mass transfer due to turbulence is considered through the use of a total diffusion coefficient, which is the sum of the molecular and turbulent contributions:

$$D_i = D_{Mi} + D_t$$

Where D_{Mi} and D_t are molecular and turbulent diffusion coefficients, respectively. The value for the turbulent diffusion is proportional to the distance from the electrodes (6) and is given by the following relation:

$$D_t = Cx^3$$

The mobility of the ions is given by the Nernst-Einstein equation.

$$u_i = \frac{D_{Mi}}{RT}$$

Properties of the system and solver

A 1-D domain has been assumed, representing the space between the two electrodes, considered as 0.05 m in this study. In the presented results, the cathode and anode are at a location of x=0[m] and x=0.05[m], respectively. The other properties of the system are given in the table below:

Table 1: Properties of the cell

Properties	value
Temperature, T	1240 K
Cryolite ratio, CR	1.5
Bath electric conductivity, Ω (15)	2.4 Ω-1.cm-1
Bath density, ρ (1)	2.059 g.cm-3
Current density, i	7500 A/m2

The sets of equations and boundary conditions are discretized and solved by the finite element method software, COMSOL Multiphysics. The maximum mesh size is 0.01 mm and the number of degrees of freedom solved is 35008.

Results and discussion

The results are presented for the behavior of different ions during the first 1000 seconds after the startup of the electrolysis process. The initial condition that prevails in the bath is such that the equilibrium condition can be considered. The concentration and flux of ions will be presented in order to illustrate the motion of these ions and the progression of their concentration with time.

Figure 1 illustrates the mass fraction of F⁻ ions near the cathode and the anode, respectively. As shown, the mass fraction of this ion near the cathode is increasing with time because of the production of F⁻ by the cathodic reaction. Once produced, this negatively charged ion is migrated and diffused away to the anode. Based on the concentration increase with time, it can be concluded that the production rate exceed the migration and diffusion fluxes. However, this tendency levels off as the concentration gradient of F⁻ ions becomes larger.

As expected, the concentration of F⁻ near the anode is lower than the bulk value because of its consumption in the anodic reaction. It also shows that the consumption rate is dominant compared to migration and diffusion mass fluxes of this ion. As a result of the

cathodic reaction, the bulk value of the F⁻ becomes larger with time, creating larger concentration gradients near the anode and explaining the increase in the mass fraction of this ion between 500 s and 1000 s.
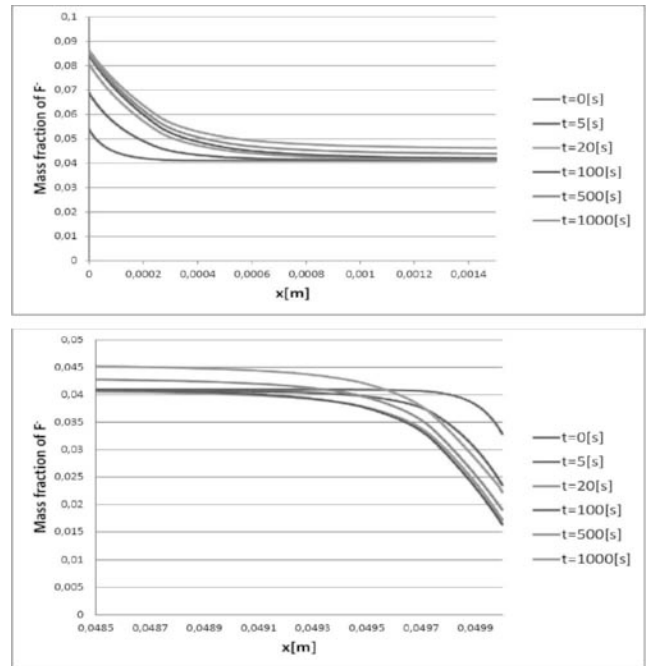

Figure 1: Mass fraction profile of F⁻ near the cathode (above) and the anode (below) for the first 1000 s.

While $Al_2OF_6^{-2}$ is participating in the anodic reaction, it is considered as a nonelectroactive ion at the cathode where only diffusion and migration takes place. The variation of concentration of this ion close to the cathode and anode is shown in figure 2. As it is negatively charged, the electric field (and migration) forces this ion away from cathode while diffusion acts in the opposite direction. This is why $Al_2OF_6^{-2}$ is found at such a low concentration near cathode. On the other side of the cell, two mechanisms are opposed. Migration and diffusion brings this ion toward the anode but it is consumed through the anode reaction. The consumption rate being higher than the migration and diffusion flux, there is depletion of this ion near the anode with time.
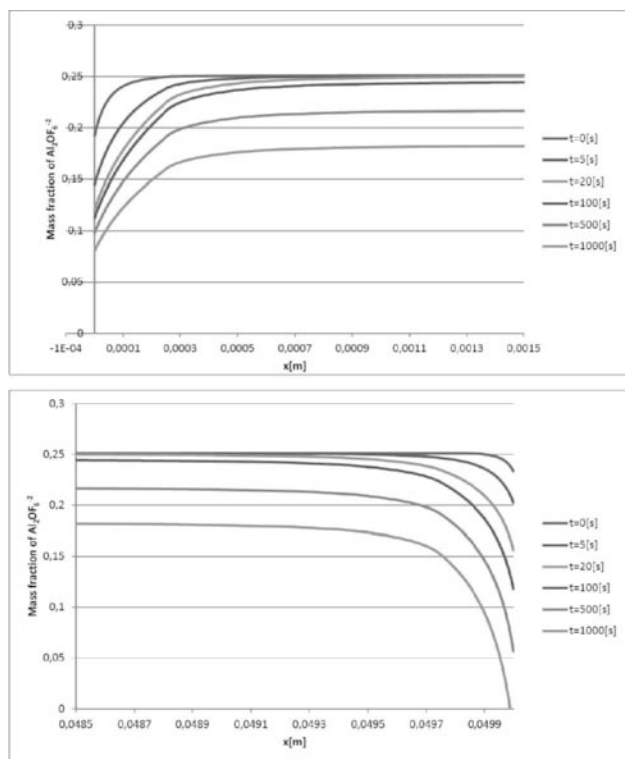
Figure 2: Mass fraction profile of $Al_2OF_6^{-2}$ near the cathode (above) and the anode (below) for the first 1000 s.

It should be noted that the effects of moving CO_2 bubbles and micro-convection below the anode has been neglected in this study. In reality, these phenomena will add additional movement of bulk, which would most probably prevent the depletion of $Al_2OF_6^{-2}$ near the anode, when the alumina concentration in the bulk is sufficient enough to sustain the production of aluminium.

Like F^-, AlF_4^- is participating in both anodic and cathodic reactions. At the cathode, the consumption and also the migration of this ion decrease its mass fraction. Near the anode, both the reaction and migration increase its concentration while diffusion mass transfer acts in the opposite direction. It is clear from figure 3 that bulk value of AlF_4^- mass fraction increases with time. This is because of the stoichiometry of the reactions. In other words, its production rate is higher at the anode that its consumption rate at the cathode.
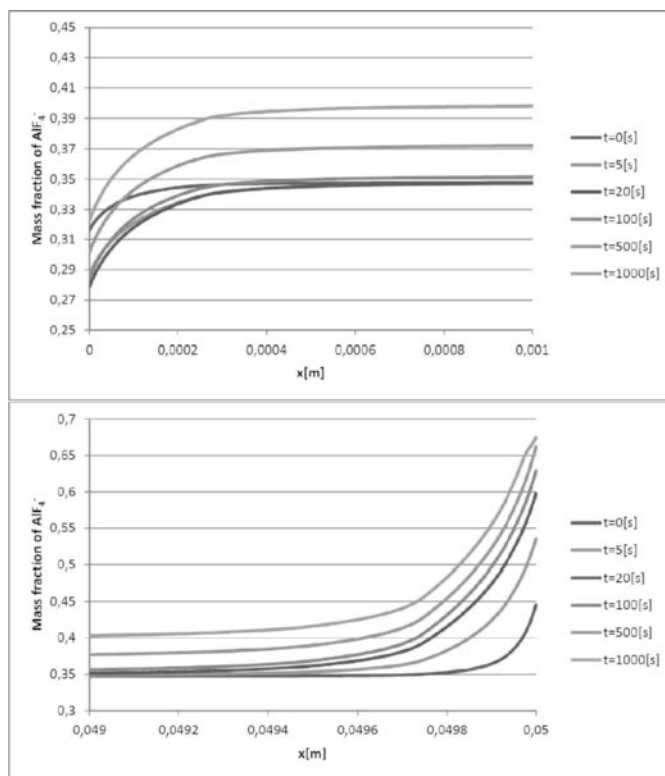

Figure 3: Mass fraction profile of AlF_4^- near the cathode (above) and the anode (below) for the first 1000 s.

The ratio of diffusion to migration fluxes provides valuable information about their relative contributions. Such a ratio is shown in figure 4 for electroactive species like AlF_4^-. For such species, in the early stages of electrolysis, the migration flux is dominant in comparison to diffusion, especially in the bulk. Shortly after the startup, the concentration gradients near the electrodes are growing, responsible for the increasing role of diffusion mass transfer with time. For AlF_4^-, the ratio of diffusion to migration is higher in the anode region because of higher concentration gradients at this location.

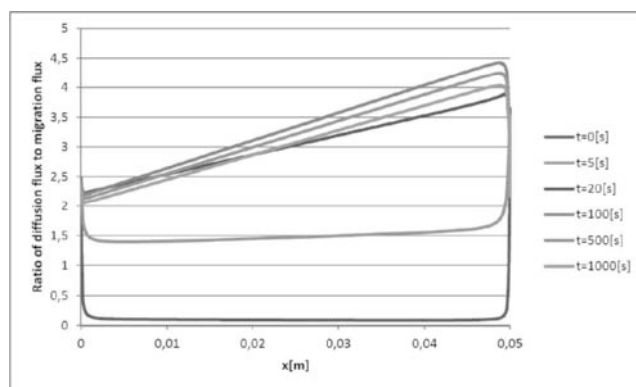Figure 4: Ratio of diffusion flux to migration flux along the cell for AlF_4^-

The diffusion to migration ratio of the $Al_2OF_6^{-2}$ is shown in figure 5. Near the cathode, this ratio takes values below or near unity, meaning that the migration plays a major role for this nonelectroactive ion. In fact, diffusion is sort of compensating the

mass transfer initiated by the migration in reaction to the presence of an electric field. On the other side of the cell, consumption of $Al_2OF_6^{-2}$ is at such a level that there is a depletion of this species near the anode. This creates a very high concentration gradient and causes the ratio of diffusion over migration to be very high in this region.
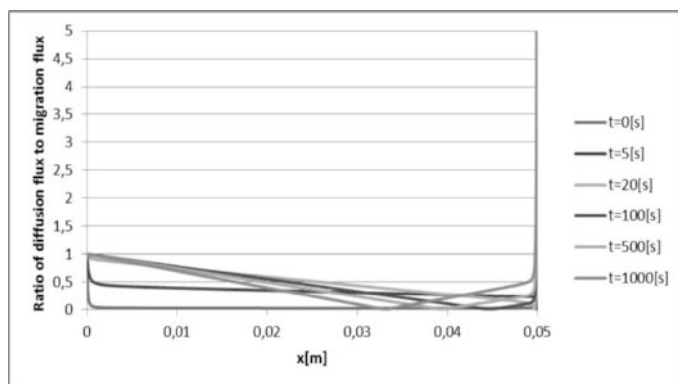

Figure 5: Ratio of diffusion flux to migration flux along the cell for $Al_2OF_6^{-2}$

For nonelectroactive ions, the diffusion to migration ratio is always below one, as shown in figure 6 for $Al_2O_2F_4^{-2}$. The mass transfer for these species is essentially driven by migration. It then creates a concentration gradient and a diffusion flux, in reaction to migration.
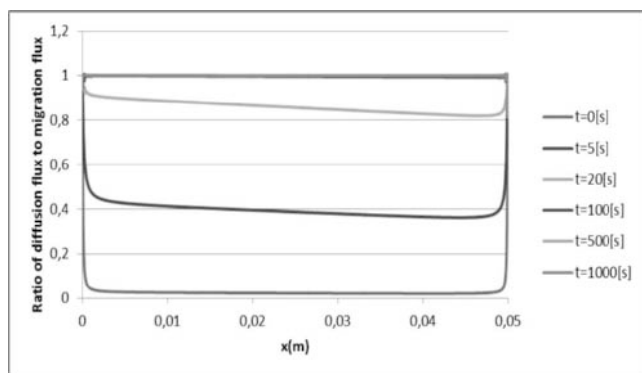

Figure 5: Ratio of diffusion flux to migration flux along the cell for $Al_2O_2F_4^{-2}$

Conclusion

The mass transfer of different ions in the NaF-AlF$_3$-Al$_2$O$_3$ molten salt has been analyzed considering electrochemical reactions, diffusion and migration as the main mechanisms of transport. The results indicate that migration plays an important role for all anions, especially for F$^-$ and $Al_2OF_6^{-2}$ that move toward anode to participate in anodic reaction. For $Al_2OF_6^{-2}$, produced by the decomposition of the alumina fed to the cell, diffusion becomes the dominant mass transfer mechanism in the region near the anode because of the presence of high concentration gradients caused by the reaction. At the cathode, the migration of $Al_2OF_6^{-2}$ is the dominant mechanism of transport. The story is similar for other electroactive ions like AlF$_4^-$. Diffusion has a considerable effect on mass transport since electrochemical reactions are responsible for large concentration gradients at both electrodes. However, the mass fluxes for nonelectroctive anions are essentially driven by the electric field force and diffusion flux is

consequently always less or equal to the migration flux. This new knowledge of the dominant mechanism of mass transfer for different ions opens up new possibilities as to control the flux of specific ions or to prevent the undesirable reactions.

References
1. Thonstad, J., Fellner, P., Haarberg, G. M., Híveš, J., Kvande, H., and Sterten, A., editor. Aluminium electrolysis. fundamentals of the Hall_Héroult process. 3rd ed. Düsseldorf,: Aluminium-Verlag; 2001.
2. K. Grjotheim, H. Kvande. Introduction to aluminium electrolysis. second edition ed. Dusseldorf: Aluminium-Verlag; 1993.
3. Zoric J, Roušar I, Thonstad J. Mathematical modelling of industrial aluminium cells with prebaked anodes part I: Current distribution and anode shape. J Appl Electrochem. 1997;27(8):916-27.
4. Zoric J, Thonstad J, Haarberg T. In: Influence on current distribution by the initial shape and position of an anode and by the curvature of the aluminum in prebake aluminum cells. Light metals: Proceedings of sessions, TMS annual meeting (warrendale, Pennsylvania); ; 1998. p. 445-53.
5. Zoric J, Thonstad J, Haarberg T. Influence of the initial shape and position of an anode and the curvature of the aluminum on the current distribution in prebaked aluminum cells. Metall Mat Trans B Process Metall Mat Process Sci. 1999;30(2):341-8.
6. Solheim A. In: Crystallization of cryolite and alumina at the metal-bath interface in aluminium reduction cells. Light metals: Proceedings of sessions, TMS annual meeting (warrendale, pennsylvania); ; 2002. p. 225-30.
7. Solheim A. In: Concentration gradients of individual anion species in the cathode boundary layer of aluminium reduction cells. TMS light metals; ; 2012. p. 665-70.
8. Gagnon F, Ziegler D, Fafard M. In: A preliminary finite element electrochemical model for modelling ionic species transport in the cathode block of a hall-héroult cell. TMS light metals; ; 2011. p. 537-42.
9. Li J, Xu Y, Zhang H, Lai Y. An inhomogeneous three-phase model for the flow in aluminium reduction cells. Int J Multiph Flow. 2010.
10. Kuzmin RN, Provorova OG, Savenkova NP, Shobukhov AV. In: Mathematical modelling of electrochemical reactions in aluminium reduction cells. WIT transactions on engineering sciences; ; 2009. p. 141-9.
11. Kuzmin RN, Savenkova NP, Shobukhov AV. Mathematical modeling of aluminum electrolysis over a long interval of time. Moscow University Physics Bulletin. 2009;64(3):294-8.
12. Zhang Y, Rapp RA. Modeling the dependence of alumina solubility on temperature and melt composition in cryolite-based melts. Metall Mat Trans B Process Metall Mat Process Sci. 2004;35(3):509-15.
13. Zhang Y, Wu X, Rapp RA. Solubility of alumina in cryolite melts: Measurements and modeling at 1300 K. Metall Mat Trans B Process Metall Mat Process Sci. 2003;34(2):235-42.
14. Zoric J, Roušar I, Thonstad J, Haarberg T. Mathematical modelling of aluminium cells with prebaked anodes part II: Current distribution and influence of sideledge. J Appl Electrochem. 1997;27(8):928-3.
15. Híveš J, Thonstad J, Sterten Å, Fellner P. Electrical conductivity of molten cryolite-based mixtures obtained with a tube-type cell made of pyrolytic boron nitride. Metall Mat Trans B Process Metall Mat Process Sci. 1996;27(2):255-61.